International Journal of Mechanical, Industrial and Aerospace Sciences
ISSN: 2517-9950
Vol:7, No:9, 2013

Computational Investigation of the Combined Effects of Yaw, Rotation & Ground Proximity on the Aerodynamics of an Isolated Wheel

T. D. Kothalawala, A. Gatto, and L. Wrobel

***Abstract*—**An exploratory computational investigation using RANS & URANS was carried out to understand the aerodynamics around an isolated single rotating wheel with decreasing ground proximity. The wheel was initially modelled in free air conditions, then with decreasing ground proximity and increased yaw angle with rotational speeds. Three speeds of rotation were applied to the wheel so that the effect of different angular velocities can be investigated. In addition to rotation, three different yaw angles were applied to the rotating wheel in order to understand how these two variables combined affect the aerodynamic flow field around the wheel.

***Keywords*—**Aerodynamics, CFD, Ground Proximity, Landing Gear, Wheel, Rotation, Yaw.

I. Introduction

THE unsteady aerodynamics around the landing gear is a problem which to date has received little attention in the aircraft industry. Although this component is a major contributor to the noise generated from an aircraft, the complexity of the design and the flow interactions makes this particular configuration very difficult to analyse and quantify accurately. The scope of this research is to carry out an exploratory analysis to understand how the flow around a single wheel behaves as an isolated configuration but also how rotation and yaw effects impact the flow field.

Fackrell [1] conducted an experimental investigation on an isolated wheel in contact with the ground. Rotation was also applied to this wheel by means of a moving floor. A range of wheel profiles were used to analyze the flow field around the wheel. Boundary layers on the wheel and ground were forced against each other at the point of contact, resulting in a positive pressure peak which was measured at C_p=2. The pressure peak was also found to extend upstream on the line of contact between the wheel and the ground. McManus & Zhang [2] also carried out a computational study with a wheel in contact with the ground. The wheel geometry used was identical to the profiles used in [1] and is the one also chosen for this study. From results obtained, stationary and rotating wheel cases were found to have a C_D of 0.48 and 0.44 respectively. In comparison, Fackrell [2] obtained a value of C_D= 0.51 which was compared to these computational results. Lift coefficient results in [2] of 0.152 & 0.156 were also found. Analysis of the flow field showed a pair of counter-rotating longitudinal vortices in the lower near wake of the wheel along with evidence of the flow separating at the top downstream the wheel. Lazos [4] also investigated the flow around a four wheel landing gear configuration. This experimental investigation indicated an area of flow separation on the first wheel to be located at 220°, reattaching thereafter on the second wheel at 30° on the 'wing' side and -35° on the 'ground' side. This phenomenon allowed a vortex to be formed in the gap between these two areas of attachment on the 'wing' side of the wheel enabling a vortex to develop. Pressure measurements carried out on the model revealed a pressure drop on the ground side corresponding to a higher velocity. A wavy and discontinuous vorticity layer also showed signs of instability at -115° on the first wheel (measured from the stagnation point). This instability in the shear layer resulted in a change of separation characteristics on the ground side of the wheel causing the flow to attach and separate at different positions. The vortex formed between the wheels was found to be a possible source of noise because when in a stationary position, the vortex will scrub turbulent eddies against the wheel's surface as it collides between the two wheels. After and from the work of Fackrell [1], it was mentioned by Thivolle-Cazat and Galleon [5] that less drag is produced from an isolated rotating wheel than from a stationary wheel in contact with the ground. Separation was noticed over the top of the wheel due to the rotation applied. The wheel rotating in contact with the ground also produces a higher pressure at the point of contact beneath the wheel but the low pressure acting over the top of the stationary wheel contributes towards a greater drag. More recently an experimental study of a wheel in free air was conducted by Zhang, Smith and Sanderson [3]. This study showed lines of separation around the top of the wheel as the air from the hub interacts with the air flowing around the wheel. The flow was forced to pass around the edges of the wheel and meet behind the wheel causing four trailing vortices.

T. D. Kothalawala, A. Gatto, and L Wrobel are with the School of Engineering & Design, Brunel University, Uxbridge, UB8 3PH, UK (e-mail: Tharaka.Kothalawala@brunel.ac.uk, Alvin.Gatto@brunel.ac.uk, Luiz.Wrobel @brunel.ac.uk).

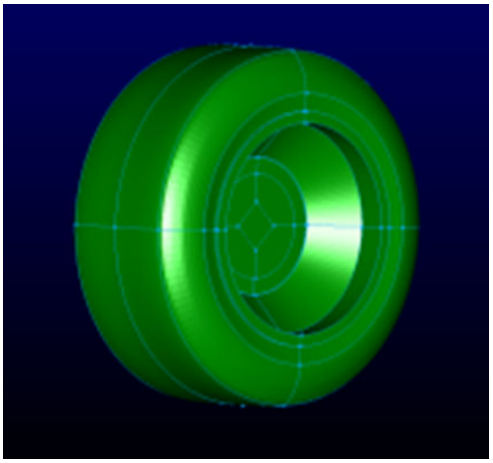

Fig. 1 Computational wheel

II. Design Methodology & Approach

A. Wheel Geometry

The wheel modeled in this study was the 'A2' configuration detailed in [1] and used in the computational results obtained in [2]. The diameter and breadth of the wheel are 0.416m and 0.191m, respectively.

B. Computational Approach

Mesh generation software was used to create the initial grid. Initially, the wheel modelled (Fig. 1) was placed in the centre of the computational grid to analyze a free air configuration. The structured grid created contained 2 million cells. Criteria to be met included; keeping the Equiangle Skewness below 0.9, keeping the Jacobians (volume of the blocks) positive and ensuring a wall spacing on the surface of the wheel corresponds to y+ value near 1.

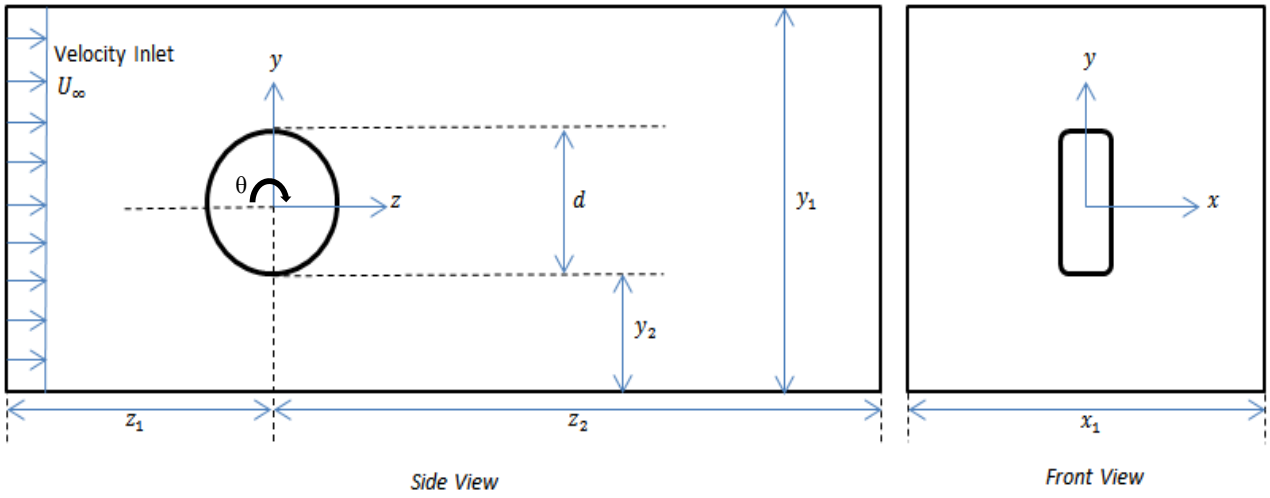

Fig. 2 Computational Domain

1. Boundary & Mesh Refinement Study

A boundary and mesh refinement study was carried out to find the most appropriate sized grid which provides a good accuracy whilst keeping the computational time to a minimum.

For the boundary refinement study, the far field boundary distance was changed by 0.5, 1.2, 1.4, 1.6 & 2 times the original grid size. From these simulation results, the values of C_L& C_D were obtained and plotted on a graph against boundary enlargement. The final boundary size chosen for the study was where C_D was within 99% of the ultimate final value of C_D.

Similarly, a mesh refinement study was also conducted. For this study, a mesh density study was conducted using grids of 1, 4 and 6 million cells. Using the same approach used for the boundary study a final mesh of over 3 million cells was chosen.

C. Computational Grid

Based on the boundary and mesh refinement study, the most appropriate sized grid consisted of over 3 million cells and a far field boundary distance 1.2 times the original grid size chosen. The final grid configuration is shown in Fig. 2. Overall, the inlet domain has a width ofx_1/d= 2.19 and a height of y_1/d= 6.04. The inflow boundary was placed at a distance of z_1/d= 6 upstream of the wheel and the outflow boundary placed at a distance of z_2/d= 18 downstream of the wheel.To understand the effect of rotation with decreasing ground proximity, the wheel was modelled closer to the ground by halving the distance from the bottom of the wheel to the ground by half in two instances, i.e. y2/d=2.52 (free air), y2/d=1.26 and y2/d=0.63. The rotation on the wheel was set to 100, 200 and 327rad/s respectively; 327rad/s being equivalent to an oncoming free stream air speed of 70m/s. These speeds were set as an anticlockwise angular velocity on the wheel (when looking in the +x direction); opposing the direction of

the oncoming flow at the top of the wheel. Yaw angles of 5, 10 and 20° were also applied to the geometry of the wheel.

D.Simulation Parameters

Both RANS & URANS methods were used for simulation in this present study. The flow around a wheel of an aircraft's landing gear is highly unsteady due to the large amount of flow interactions. Therefore the unsteady (URANS) solver is expected to provide results to a better level of accuracy compared to the steady (RANS) solver. Comparisons between RANS & URANS can also be compared directly.

1. Turbulence Modelling

The turbulence model used for this study is the two equation Realizable k-ε model, due to its simplicity, accuracy and use in previous studies [6]. This model is well known for working with boundary layers, strong and adverse pressure gradients, separation, rotation and recirculation; all of which are involved in the flow around a landing gear. This model has also been used in similar studies with reasonably good accuracy [2].

2. Boundary Conditions

The inlet free stream velocity (U∞) was kept at 70m/s giving a Reynolds number of 1.9×10^6. The inlet boundary condition was set as a velocity inlet and the outlet boundary condition was set as a pressure outlet with a gauge pressure of zero. A symmetry boundary condition was used for the wheel and the walls of the computational domain.

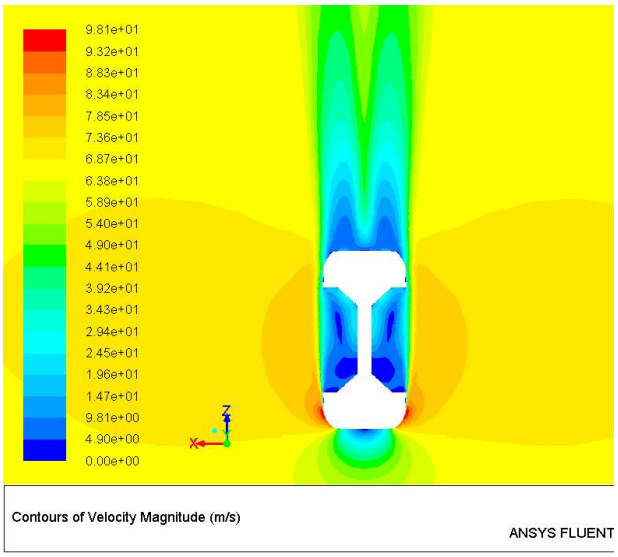

Fig. 3 Velocity Magnitude Contour plot across centerline of wheel in free air

3. Solution Settings

During the steady state solution in the RANS condition, the simulations were run until the residuals converged by up to five orders of magnitude. In some simulations, the flow did not converge for a few thousand iterations but had achieved a steady value. In this case, the simulation was terminated. For the unsteady solver, a time step of 0.01 was used with 20 iterations per time step. For these cases, the model was simulated until the residuals converged by to three orders of magnitude.

III. Results

Initially the wheel was simulated in free air with no rotation applied with the flow around the wheel being symmetrical about the centreline of the wheel shown in Fig. 3. As the air flows around the sides of the wheel, the velocity increases from 70m/s to 98m/s, representing an acceleration of the flow as the air travels around the curved edges of the wheel. This was also experienced in [2]. When the hub of the wheel is approached, the air is pulled inside the hub and circulated because of the inability to flow straight past the wheel due to the shape of the hub. Soon after the air reaches the back of the wheel, wakes are formed behind the wheel. As the wheel is lowered towards the ground, there is a significant increase in the coefficient of drag (C_D) and small variations in the coefficient of lift (C_L). These values of C_D and C_L are presented in Table I, according to the rotary speed on the wheel with decreasing ground proximity simulated in RANS and URANS conditions. Table I indicates that as the wheel gets closer to the ground, the drag increases using the RANS method by 23%. The URANS simulations show a similar but stable trend when compared to the RANS results; though this is expected as modelling an unsteady flow on a steady solver should show some instability.

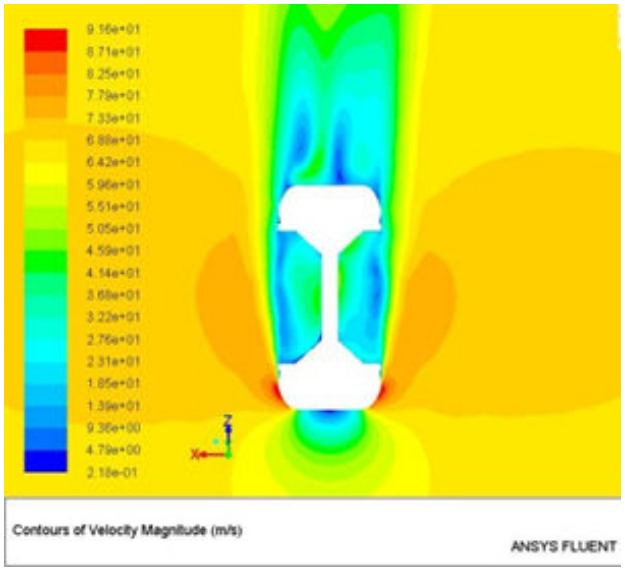

Fig. 4 Velocity Magnitude Contour plot across centerline of wheel in free air rotating at 100rad/s

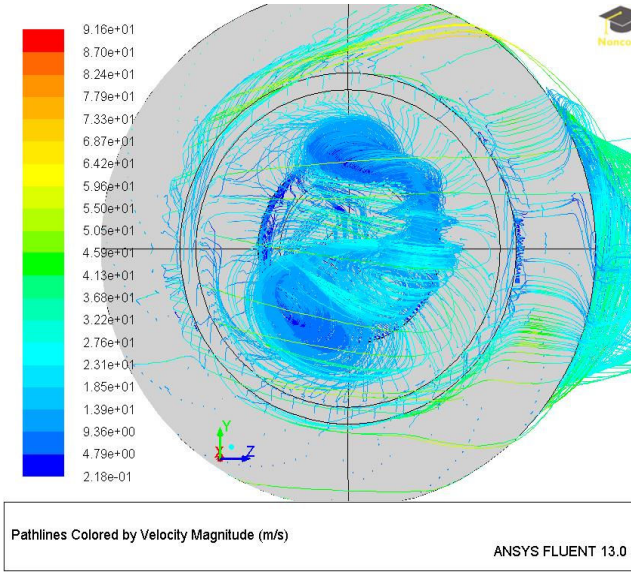

Fig. 5 Pathlines of Velocity Magnitude inside hub in +x direction

As a rotatory speed of 100rad/s is applied on this wheel in free air, a similar but less uniform flow is experienced around the wheel. Fig. 4 shows this result indicating a faster flow of 45m/s inside the hub area compared to the stationary wheel. Fig. 5 also shows a vortex being formed inside the hub section caused by the interaction between the circulatory flow in the hub and the rotation of the wheel. As the speed of rotation increases furthermore to 200rad/s and 327rad/s, with the wheel decreasing in ground proximity, C_D continues to increase. Fig. 6 indicates that whilst having a value of C_D =0.41 in the URANS stationary and free air conditions, C_D increases significantly by 51% when the wheel is at a distance of 0.26m to the ground with rotational speed of 327rad/s.The coefficient of drag experienced in [3] was0.29; which is roughly half the value obtained in this simulation (C_D=0.41) for the stationary wheel using URANS conditions. In steady conditions the value of $C_D$is 0.21, but compared to [3], this result represents a decrease of 38%. McManus and Zhang [2] also obtained a value of C_D=0.44 for their rotating wheel in contact with the ground and was in general agreement with C_D=0.51 from the experimental results in [1]. The values of C_D obtained in this study varies by up to 20% when compared to [2], however the wheel in [1] and [2] was modelled in contact with the ground. Therefore it will be of interest to see if a similar value is to be achieved once the wheel in contact with the ground is to be modelled and simulated.

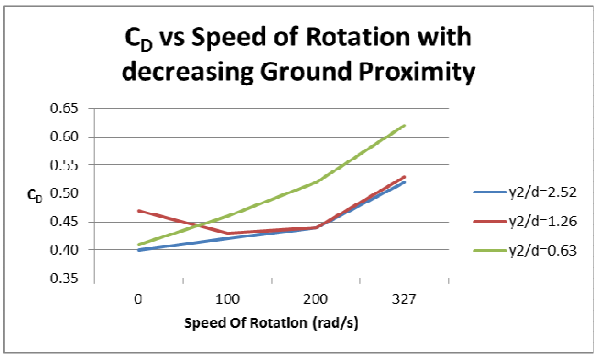

Fig. 6 Graph of drag coefficient against the speed of rotation with decreasing ground proximity

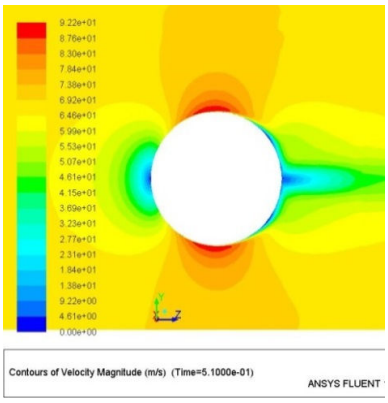

Fig. 7 Contour plot of velocity magnitude across centerline of wheel in free air with no rotation

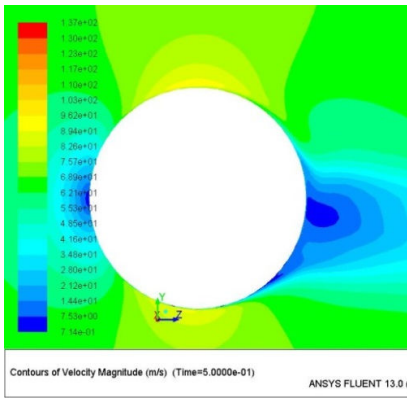

Fig. 8 Contour plot of velocity magnitude across centerline of wheel in free air, rotating at 327rad/s

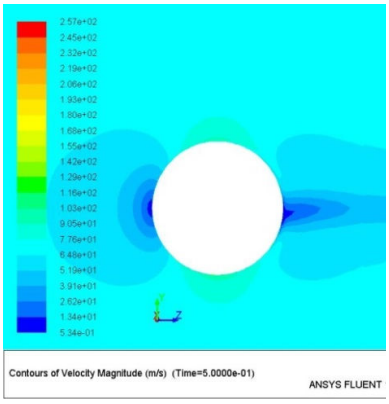

Fig. 9 Contour plot of velocity magnitude across centerline of wheel at y_2/d=0.63, rotating at 327rad/s

TABLE I
VALUES OF LIFT AND DRAG FORCE COEFFICIENTS FOR WHEEL WITH DIFFERENT SPEEDS OF ROTATION WITH DECREASING GROUND PROXIMITY IN BOTH RANS & URANS METHODS

	$y_2/d=2.52$				$y_2/d=1.26$				$y_2/d=0.63$			
	RANS		URANS		RANS		URANS		RANS		URANS	
	C_D	C_L	C_D	C_L	C_D	C_L	C_D	C_L	C_D	C_L	C_D	C_L
Stationary	0.21	0.04	0.41	0.00	0.22	0.00	0.46	0.00	0.26	-0.01	0.41	0.00
100rad/s	0.41	-0.01	0.42	0.00	0.48	-0.01	0.43	-0.04	0.52	0.07	0.46	0.00
200rads	0.50	0.12	0.44	0.03	0.45	-0.05	0.44	-0.03	0.55	-0.01	0.53	-0.03
327rad/s	0.51	-0.02	0.52	0.16	0.53	-0.08	0.53	-0.07	0.62	-0.09	0.62	-0.07

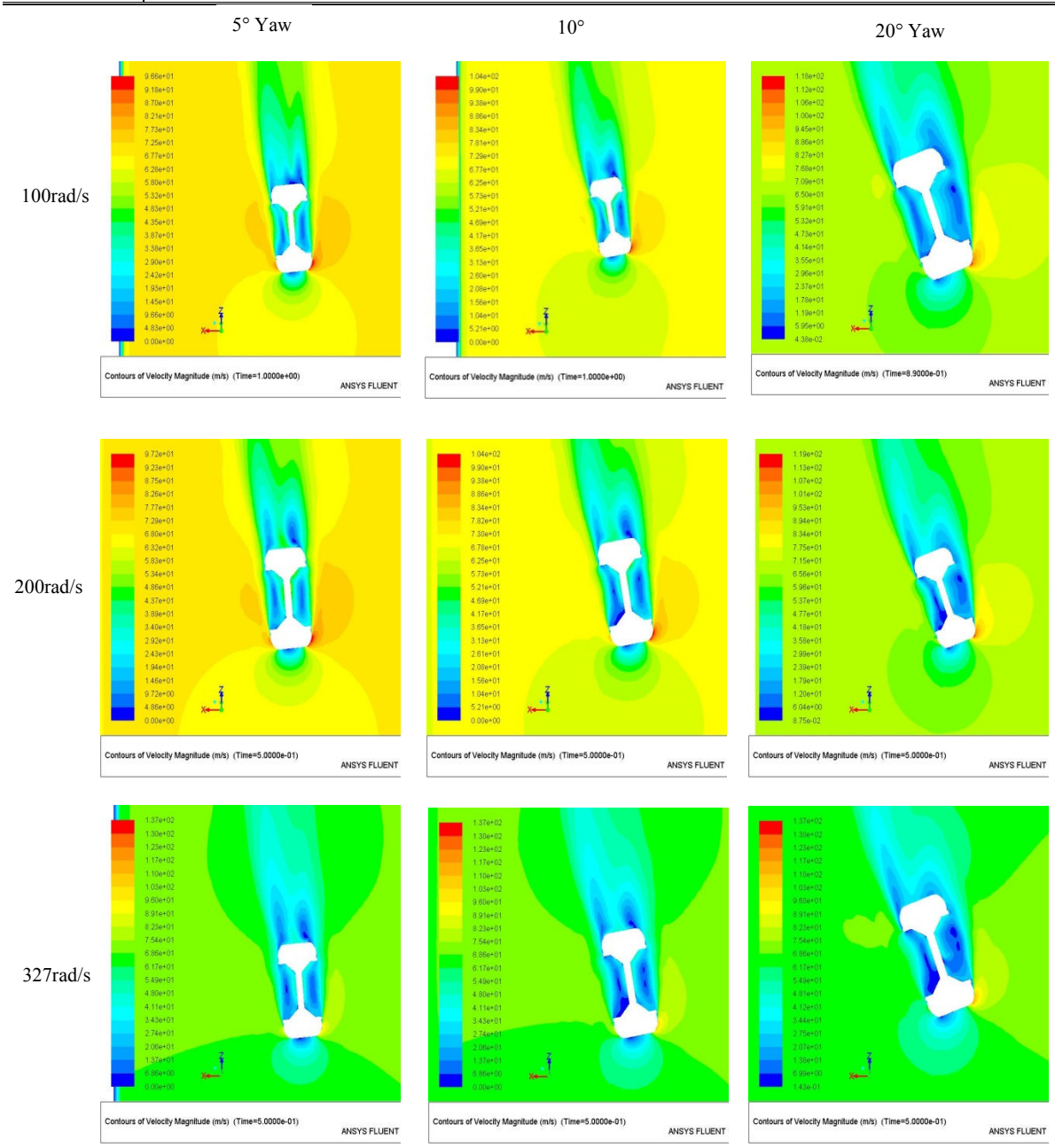

Fig. 10 Velocity Contour plots across centerline of wheel showing flow variations for different rotating speeds with added yaw angle in free air

Comparing RANS and URANS, Table I shows an interesting pattern; the RANS produced results of C_D 50-60% less the value of that obtained from the URANS method whilst the wheel was stationary; however the results between RANS

& URANS had a variation of up to 10% once rotation was applied on the wheel. This indicates that when rotation was added on the wheel, the RANS & URANS gave more similar results. Figs. 7 and 8 show the side view (+x direction) contour plots of velocity magnitude in free air with no rotation and with a rotational speed of 327rad/srespectively. As the speed of rotation increased, the value of C_D and the size of the wake behind the wheel increased due to the lower pressure; C_P=0.1 and -0.25 directly behind the wheel with no rotation and 327rad/s of rotation respectively. Accordingly with these values of C_P, the mean velocities behind the two wheels are 7m/s and 2m/s respectively. This shows that as the rotation increased up to 327rad/s, the pressure and velocity of the flow directly behind wheel decreased causing a larger wake. However once the wheel rotating at 327rad/s was lowered by 1.9$d$closer to the ground (Fig. 9), drag increased by 19% and the size of the wake decreased. The values of CL in Table I show negative values as the wheel decreases in ground proximity. This indicates that the wheel is being 'sucked' towards the ground but as [2] has C_L=0.16 in contact with the ground, there should be a point where as the wheel decreases in ground proximity, the value of C_L is positive and the wheel is pushed up.

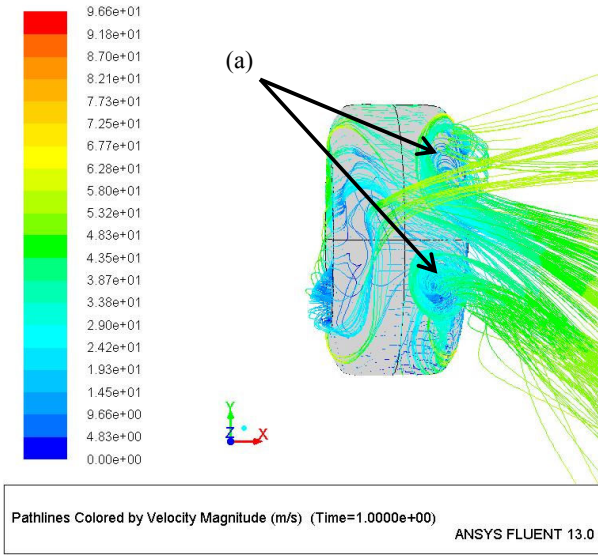

Fig. 11 Pathlines of velocity magnitude behind the wheel in free air rotating at 100rad/s with 5° yaw

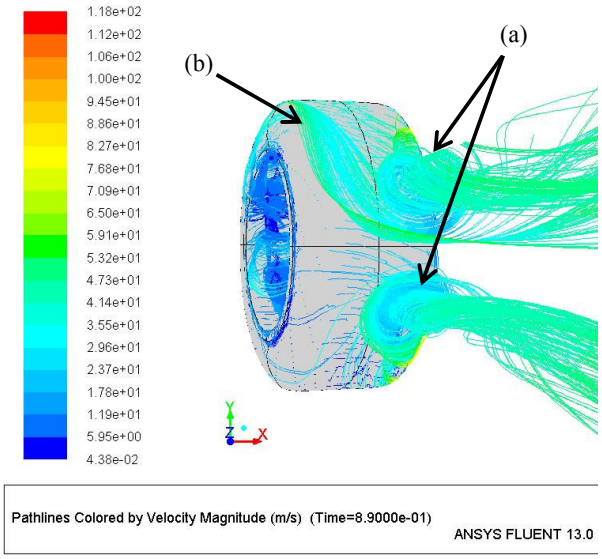

Fig. 12 Pathlines of velocity magnitude behind the wheel in free air rotating at 100rad/s with 20° yaw

With the applied effect of yaw, the velocity contour plots across the centerline of the wheel can be visualized in Fig. 10. As the yaw angle is increased and the flow travels on to the sides of the wheel, the air on the left side of the wheel is obstructed by the edge of the hub at the back. This causes the air to take the shape of the hub and travel inside. As a result, the air is circulated in the hub cavity. As the speed of rotation increases to 327rad/s, the mean velocity of the air, as it first interacts with the front of the wheel, increases by 43%. Figs. 11 and 12 show the wheel in free air with a yaw angle of 5° and 20° respectively. A pair of vortices can be seen to extend off the shoulders on either side of the horizontal centerline of the wheel, marked (a) in Figs. 11 and 12.The air is separated off the top left edge off the wheel as marked (b) in Fig. 12, and interacts with the top vortex forming a wake.

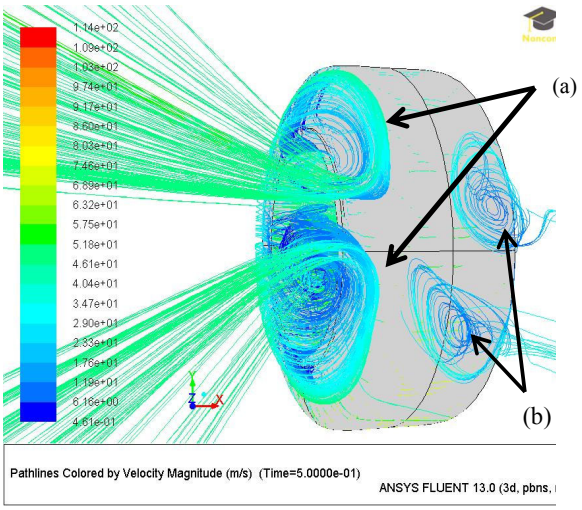

Fig. 13 Pathlines of Velocity magnitude behind whilst rotating at 100rad/s with 20° yawat y2/d-0.63

Fig. 13 shows the URANS wheel at its closest point to the ground rotating at 100rad/s with 20° yaw. Two vortices are formed on the left of the wheel (right side of figure as it is a rear view). The wake on the left in Fig. 12 is created by the circulated air being forced out of the hub and attaching to the flow separated off the shoulders of the wheel as shown in Fig. 13 (a).

As the rotary speed of the wheel is increased to 327 rad/s, the wake on the right side of the wheel (left in Fig. 14 as it is a rear view), shows the wake being extended out but from the hub instead of the shoulders of the wheel compared to Fig. 13 which was rotating at a lower speed of 100rad/s. This is more evident on the top view of the wheel as shown in Fig. 15. Two vortices are also formed at the back of the wheel shown in Fig. 13 (b) whilst rotating at 100rad/s, but only rotating at 327 rad/s (Fig. 14 (a)) the circulated air behind the wheel is pulled together and forms a larger vortex.

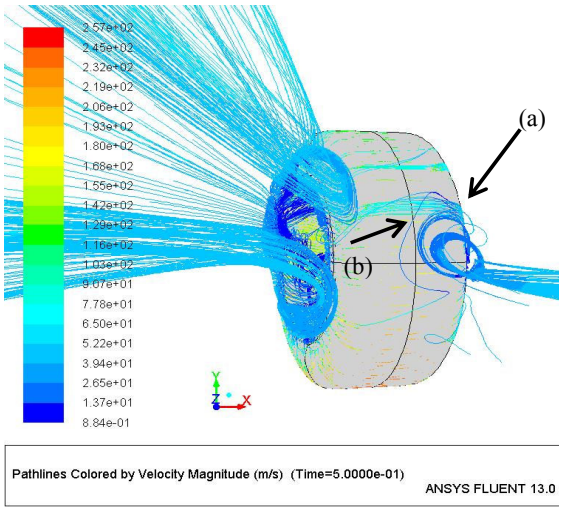

Fig. 14 Pathlines of Velocity magnitude behind wheel rotating at 327rad/s at y_2/d-0.63 with 20° yaw

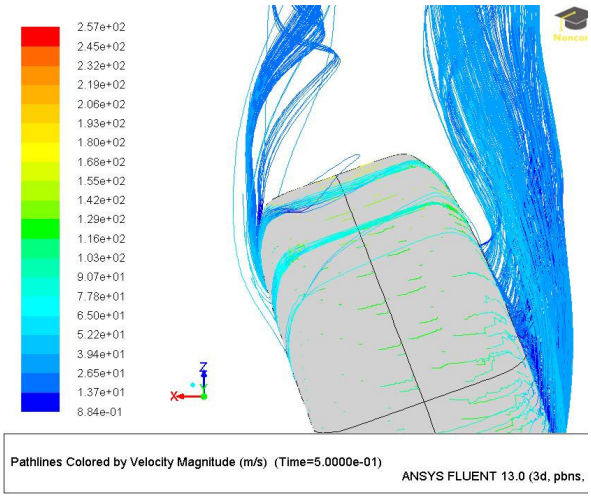

Fig. 15 Pathlines of Velocity magnitude, showing a top view, whilst rotating at 327rad/s with 20° yawat y2/d-0.63

IV. Conclusion

Results for an isolated wheel in contact with the ground, for a wheel with applied rotation indicate recirculation in the wake in the lower region behind the wheel. A similar formation was seen in this study in the wake behind the wheel as seen in Fig. 12. As a direct comparison, a drag force coefficient (C_D) of 0.43was experienced in [2] for the computational study in contact with the ground and a C_D of 0.51 from the experimental results in [1].However, C_D= 0.46 was found in this study. In this study however the wheel was only modelled close to the ground. Nevertheless, this is an encouraging result with values of C_D varying by only up to 10%.Results also showed that as the wheel remained in free air, the increase in rotational speed from 100rad/s to 327rad/s formed a bigger wake due to the reduced velocity and pressure behind the wheel causing an increase in drag. However as the wheel rotating at 327rad/s was modelled closer to the ground by $1.9d$, the drag increased by 19%. Additionally, the effect of increasing yaw angle with rotation revealed that as the yaw angle increases in free air, the flow is separated at θ=130° and θ=210° on the wheel. However, when modelled at 327rad/s with 20° yaw and lowered to the ground by $1.9d$, the flow from the hub extends to form a wake towards the right (when looking in the +z direction). Similarly, the area of reduced velocity and pressure at θ=170°, behind the wheel, reveals the flow being pulled and joined to the wake formed on the left of the wheel.

References

[1] Fackrell J.E., "The Aerodynamics of an Isolated Wheel Rotating in Contact with the Ground," Ph.D. thesis, University of London, U.K.., 1974.

[2] McManus J. and Zhang X., "A Computational Study of the Flow Around an Isolated Wheel in Contact With The Ground", ASME, Vol. 128, May 2006, pp. 520-530.

[3] Zhang X., Ma Z., Smith M. and Sanderson M., "Aerodynamic and Acoustic Measurements of a Single Landing Gear Wheel", AIAA, 19th AIAA/CEAS Aeroacoustics Conference, May 2013.

[4] Lazos B. S., "Mean Flow Features Around the Inline Wheels of Four-Wheel Landing Gear", AIAA, Vol. 40, No. 2, February 2002, pp. 193-198.

[5] Thivolle-Cazat E., Gilliéron P., "Flow analysis around a rotating wheel", 13th Int Symp on Applications of Laser Techniques to Fluid Mechanics, June 2006, Paper 1030.

[6] Ansys Fluent User Guide, Ansys Inc, Release 13.0, November 2010, pp. 645-646.